8

Pulsed Full-Color Digital Holography with a Raman Shifter

Percival Almoro, Wilson Garcia and Caesar Saloma
National Institute of Physics, University of the Philippines
Diliman, Quezon City,
Philippines

1. Introduction

Holography deals with processes involving the transformation of waves by interference structures that are formed when coherent electromagnetic waves interact with matter (Andreeva, 2002). As an optical technique it was introduced in the seminal works of Gabor, Leith, Denisyuk and others in the 1960's (Benton, 2005). By succeeding to reconstruct the complete wave (full amplitude and phase information), holography yields depth information of a volume (three-dimensional) scene.

The main goal of holography in imaging is to reconstruct wavefronts from 3-D colored and moving objects in real time. Sustained success however, is still hampered by a number of technical hurdles that need to be overcome. Full-color reconstruction requires a multi-wavelength light source and a wide bandwidth light-sensitive recording medium. Conventional color holography utilizes three separate continuous-wave (CW) lasers as illuminator which is more expensive and difficult to operate and maintain. The narrow temporal bandwidth of CW lasers also restrict their applications only to holographic imaging investigations involving stationary objects.

Here we discuss the use of the hydrogen Raman shifter as a pulsed color holographic light source. The Raman shifter is an attractive holographic light source because it is pulsed, compact, inexpensive, and multi-wavelength (Almoro et al., 2004; Almoro et al., 2007). Pulsed color light sources extend the range of possible applications of color holography to fast moving objects and rapid events. Due to significant advances in photodetector and computer technology, holograms can now be recorded with high-resolution digital cameras and reconstruction could be carried out numerically in a fast manner (Schnars & Jüptner, 2002).

Digital holography is suitable for industrial applications since it does not involve the cumbersome development of photographic films. In full-color digital holography, a minimum set of three holograms are captured corresponding to the primary color channels (i.e., red, green and blue color channels). For a proper fit of the superposition of the reconstructions, it is important to characterize and control the wavelength dependences of the image size, lateral resolution and depth of focus. These image variations result in the dispersion of the color hologram reconstructions making the final image blurred and unacceptable. Here we discuss the experimental evidence of the said effects and describe a technique to control the chromatic dispersion of full-color holograms.

2. Basic principles

2.1 Pulsed full-color digital holography

2.1.1 Digital holography

In conventional digital holography, a test object is illuminated using a CW monochromatic light and the recorded hologram is reconstructed in a computer (Schnars & Jüptner, 2002). Numerical reconstruction is achieved by calculating the diffraction of the monochromatic light incident on the hologram through a diffraction formula. The derived complex amplitude is then used to plot the intensity or phase distributions at any given plane. A three-dimensional (3D) image of a volume scene is generated from a stack of 2D intensity distributions. An unwrapped phase distribution may also be used to depict the surface shape of an object or the internal variations in the refractive index. In addition, phase distributions corresponding to different states of the test object may be compared and used to study changes in the physical state of the object or sample (Schnars & Jüptner, 2002).

Applications of digital holography have found their way in optical metrology, 3D microscopy and object recognition. In optical metrology, the reconstructed phase is used to detect material defects (Schulze et al., 2003) and to determine material properties such as the Poisson ratio, Young's modulus and thermal expansion coefficient (Seebacher, 2001). Digital holographic microscopy has been applied in the imaging of biological specimens (Zhang & Yamaguchi, 1998) and micro-optical elements (Colomb, 2010). Direct access of the complex amplitude of the reconstructed object beam allows for a more versatile discrimination of dissimilar 3D objects (Javidi & Tajahuerce, 2000).

The maximum resolution of the reconstructed image depends on the CCD pixel pitch. High-end CCD cameras that are now in the market have a pixel pitch of about 3.5 microns. The applications of digital holography are limited by the properties of the available light source. For the investigations of colored objects, a multi-wavelength light source with its wide spectral bandwidth is desirable since it enables us to sample the color information of the object in a single setting. For the investigations of dynamic objects and events, a pulsed light source is necessary.

2.1.2 Pulsed holography

Pulsed lasers extend the applications of holography to fast moving objects and transient events (Mallick, 1975). Due to the short illumination time of a pulsed laser (typically 10^{-9} second), object movements are literally frozen and the measurement resolves the rapid deformations of samples undergoing rapid kinetics. Ruby lasers (wavelength, λ = 694 nm) (Wedendal & Bjelkhagen, 1974) and Nd:YAG (λ = 532 nm) (Bates,1973) lasers, both noted for their long coherence lengths, are the commonly used pulsed lasers. Primary consideration for their popular use is the spectral sensitivity of the available holographic films which overlap with their emission wavelengths.

The advantage of pulsed holography is clearly demonstrated in applications where it is impossible for the test object to be stationary. Pulsed digital holography has been used to carry out measurements of micro-deformation occurring on the object undergoing unsteady vibrations (Pedrini, et al., 2002). Another practical application of pulse digital holography has been in the investigation of the dynamic phase change in an arc discharge (Liu, et al., 2002). Pulsed holography has also been combined with endoscopy, making the technique more compact and adaptable to industrial setting (Pedrini, et al., 2003).

The experimental issues against pulsed lasers are the aberrations and poor spatial distribution of the beams (Leith et al., 1991; Gustafsson, 2000). Degradation in the images during optical reconstructions in pulsed film holography is addressed by the use of anamorphic optics and an inter-channel coupling filter (Leith et al., 1991). For pulsed digital holography, the time between successive pulses limits the temporal resolution for hologram recording.

2.1.3 Full-color holography

Full-color holography involves the use of a multi-wavelength light source in the recording of color holograms and the subsequent superposition of the colored reconstructions. Any color in the visible spectrum is represented as a weighted linear combination of the three channel outputs that represent the primary-color channels of red (*R*), green (*G*) and blue (*B*). The red color aspects or portions of the object reflect or transmit only the red component of illumination beam. Other object colors reflect certain proportions of *R*, *G* and *B*. For example, yellow reflects equal proportions of *R* and *G* components of light, demonstrating the color addition during recording. Combined with the 3D effect, full-color holography adds realism to the reconstructions especially in imaging applications.

Full-color film holography was utilized in constructing replicas of full-color art works such as oil paintings (Bjelkhagen & Vukicevic, 2002). The quality of the reconstructions in full-color holography is improved by reducing the undesirable speckle artefacts that remain even with the use of a multi-wavelength light source (Harthong, et al., 1997). In optical metrology, a multi-wavelength light source enables measurements with variable resolution. During reconstruction in holographic interferometry, the zeroth-order fringe which indicates the reference undeformed region can be identified because of its white color that results from superposition of the primary colors used (Desse, et al., 2002; Jeong, 1999; Demoli, et al., 2003). Implementation of full-color holography has been constrained by several experimental issues. During recording, the first issue concerns with finding a suitable light source. The factors that should be considered are the range of colors, coherence lengths and relative intensities of the laser lines used. The range of colors of the reconstructions can be assessed based on the *CIE* chromaticity diagram for a given set of wavelengths (Bjelkhagen, 2002; Kubota, 2001; Peercy & Hesselink, 1994).

Four or more wavelengths provide the best color reproduction (Kubota, 2001; Peercy, 1994). One possible solution to the problem of limited coherence is the introduction of an intra-cavity Fabry-Perot etalon in the laser light source (Lin & LoBianco,1967). Previous investigations on the sampling characteristics of the holographic process have suggested using sets of wavelengths and relative intensities for color holography to improve color reproduction (Peercy & Hesselink, 1994).

The second issue in film holography recording is the spectral sensitivity of the holographic emulsion. Recording of color holograms could be achieved with two composite films (Kubota & Ose, 1979; Kubota, 1986) with sensitivities in red and blue-green or by using a single panchromatic broadband film (Bjelkhagen, 2002).

In the reconstruction in film holography the critical issues are the color shift due to emulsion shrinkage, wavelength dependence of magnification and location of the image, and the "cross-talk" or spatial overlap of the various color reconstructions resulting in a blurred image. Color shift may be addressed by chemical treatment of the holographic films (Lin & LoBianco, 1967). To achieve acceptable fit of color reconstructions, the magnifications and

locations could be adjusted using various geometry and laser sources during optical reconstruction (Olivares-Perez, 1989). The Lippman configuration has been able to address sufficienty unwanted crosstalk in film holography (Kubota & Ose, 1979). It utilizes the strict Bragg wavelength selectivity in volume reflection holograms.

The first demonstration of full-color digital holography (FCDH) was achieved using CW Helium Cadmium white light laser with outputs in the 442, 538, and 636 nm (Yamaguchi et al., 2002). The three hologram channels that were produced by the *R*, *G* and *B* channels contain all the essential information about the color of the object. To reconstruct the image of the colored object, one applies the Fresnel method to each of the holograms using the respective recording wavelengths. The grayscale images obtained from the intensity plots of the three-color channels were rendered with the corresponding color equivalents based on the proportions of the intensities of the illumination beams and the spectral sensitivity of the CCD camera (Yamaguchi et al., 2002). Finally, the *R*, *G* and *B* reconstructions were superimposed to produce a white-balanced full color image as viewed in the computer monitor.

Unlike full-color film holography, FCDH is not susceptible to the unwanted effects of emulsion shrinkage, cross talk, and limited spectral sensitivity. Color image dispersion remains an attendant issue during reconstruction that arises from the wavelength dependence of the image size, lateral resolution and depth of focus resulting in a smeared image.

2.1.4 Control of chromatic dispersion

The Fresnel method of digital hologram reconstruction which is applicable for large recording distances could be implemented via a discrete fast Fourier transform algorithm (Garcia et al., 1996). The scaling factor between the pixel sizes Δx in the hologram plane (considered as spatial domain) and $\Delta \tilde{x}$ in the image plane (or the spatial frequency domain) depends on the wavelength λ of the light source and the image distance z (Garcia et al., 1996):

$$\Delta \tilde{x} = \frac{\lambda z}{N \Delta x} \tag{2.1}$$

where $N\Delta x$ is the hologram size or the dimension of the CCD chip. The image size of the reconstruction varies for holograms recorded at different wavelengths and focused at different image distances. Longer wavelengths and a farther image distance result in a large value for $\Delta \tilde{x}$.

Because $\Delta \tilde{x}$ represents a range of spatial frequencies, the entire spatial frequency spectrum of the hologram then can be represented by a fewer number of pixels. Fewer pixels implies a smaller reconstructed image for holograms recorded using longer λ values. The lateral resolution of the reconstructed image varies with λ. Since a reconstructed image from holograms that are recorded at shorter λ's (and closer image distances) are bigger and more details are displayed, it will feature a higher lateral resolution. The depth of focus or longitudinal (axial) resolution of the reconstructions is proportional to λ and is inversely proportional to the square of the effective numerical aperture. Hence, reconstructions that are obtained with shorter λ's have shallower depths of focus. Variances in the image size, lateral resolution and depth of focus of the primary color reconstructions result in chromatic

dispersion. Compensation for chromatic dispersion is important for proper full-color overlay - failure to compensate results in a blurred image. A summary of the dependence of holographic image size, resolution and depth of focus on wavelength and distance is shown in Table 2.1.

Image parameters	Wavelength (λ)	Recording/Reconstruction Distance
Size	Longer λ, smaller size	Farther distance, smaller size
Resolution	Longer λ, lower resolution	Farther distance, lower resolution
Depth of focus	Longer λ, larger DoF	Farther distance, larger DoF

Table 2.1. Dependence of image parameters on wavelength and distance

A method for controlling chromatic dispersion in FCDH was demonstrated using two CW lasers of different wavelengths (Ferraro, 2004). The effects of varying sizes of the reconstructions from the color holograms were compensated by resizing the holograms based on the ratio of wavelengths for a fixed image distance using the relation (Ferraro, 2004):

$$N_2 = \left(\frac{\lambda_2}{\lambda_1} \right) N_1 \tag{2.2}$$

where N_1 and N_2 are the original and resized hologram dimensions, respectively. λ_2 and λ_1 are the longer and shorter wavelengths, respectively.

For example, consider two holograms with dimensions 480 x 640 pixels, one is recorded in red (λ_2 = 636 nm) and the other in green (λ_1 = 503 nm). To equalize the image pixel size for the red and green reconstructions, augment the red hologram by padding the matrix with zeros in both horizontal and vertical directions. Hence, the new dimensions for the red become 734 x 979 pixels. Upon application of the Fresnel method on the resized red hologram at the same image distance z as in the green hologram, the image sizes of the reconstructions from both red and green holograms are equalized. We employ similar procedure for image resizing with one major difference – the image distance is not fixed. A summary of the imaging equations for single-color holography is provided by Goodman (1996).

The following imaging condition is pertinent in FCDH: if the recording and reconstruction wavelengths are the same then the coordinates of the image depend only on the coordinates of the object position, location of the point reference beam and location of the point reconstruction beam. Thus, images of the same object that are reconstructed from primary color holograms are located at the same coordinates if and only if the coordinates of the point reference and reconstruction beams are the same.

Upatnieks presented similar imaging relations and stressed the effects of light source on the quality of reconstructions (Upatnieks, 1979). Exact image formation without size change and aberration requires that the wavelength for recording and reconstruction be the same and the curvature of the reconstruction wave is a replica of the original reference beam or an exact conjugate of it. During computer reconstructions of digital holograms, it is convenient to approximate the reconstruction beam as a plane wave at normal incidence to the

hologram and with the same wavelength as the recording beam. Such a numerical reconstruction beam, however, does not always satisfy the curvature requirement for the reconstruction wave.

The image position of the reconstruction usually differs from object position. Although not a serious issue in single-color holography it becomes critical in FCDH. The wavelength dependence of the beam divergence and chromatic aberrations alter the positions of the reference and illumination beams leading to wavelength-dependent variance between image and object distances. Consequently, the reconstructions from the primary color holograms of the same object are focused at different image distances. The exact amounts of displacements between the color reconstructions are normally difficult to determine since they are influenced by the specific optical elements that are used in the FCDH system. Here, we describe a technique to minimize the chromatic dispersion using the best-focused image distance during the reconstruction of the color hologram channels.

2.2 Stimulated Raman Scattering

Stimulated Raman scattering (SRS) is an inelastic scattering effect whereby an incident photon with frequency ω_p is absorbed by a molecule in the ground state. This causes the molecule to be excited to a virtual state. A second incoming photon can stimulate this molecule to relax to the ground state or to the first excited (vibrational, rotational, or vibrational-rotational) state (Garcia et al., 2002). If the Raman transition involves vibrational energy levels only, the process is known as stimulated vibrational Raman scattering (SVRS). SVRS generates photons shifted by the vibrational Raman frequency ω_{vib}. For H_2, ω_{vib} = 4155 cm^{-1}. By using a linearly polarized 532 nm pump, SVRS can generate the following vibrational Stokes lines: S_{10} = 683 nm, S_{20} = 953.6 nm, S_{30} = 1579.5 nm, …, and the following vibrational anti-Stokes lines: AS_{10} = 435.7 nm, AS_{20} = 368.9 nm, AS_{30} = 319.9 nm, … . If the transition occurs between the rotational energy levels at a single vibrational energy level, the process is known as stimulated rotational Raman scattering (SRRS).

In SRRS the photons generated are shifted by the rotational Raman frequency ω_{rot}. For H_2, ω_{rot} = 587 cm^{-1}. An elliptically polarized 532 nm pump can generate, via SRRS in H_2, the following rotational Stokes lines: S_{01} = 549.1 nm, S_{02} = 567.4 nm, S_{03} = 587.0 nm, … and the following rotational anti-Stokes lines: AS_{01} = 515.9 nm, AS_{02} = 500.7 nm, AS_{03} = 486.4 nm, …, . If the Raman medium has both vibrational and rotational excited states, as in the case of H_2, a photon shifted by both ω_{vib} and ω_{rot} can be generated via the vibrational-rotational Raman effect. This process can generate the following vibrational-rotational Stokes lines: S_{10} – AS_{02} = 632.3 nm, S_{10} – AS_{01} = 656.7 nm, S_{10} – S_{01} = 711.5 nm, S_{10} – S_{02} = 742.5 nm, … and the following vibrational-rotational anti-Stokes lines: AS_{10}- S_{02} = 459.2 nm, AS_{10}- S_{01} = 447.1 nm, AS_{10}- AS_{01} = 424.8 nm, AS_{10}- AS_{02} = 414.5 nm, AS_{20}- S_{01} = 377.1 nm, AS_{10}- AS_{01} = 361.1 nm, ….

3. Experiments in full-color digital holography

3.1 The light source

Figure 1 presents the schematic diagram of the experimental setup for pulsed FCDH which consists of three main sections: 1) Pulsed multi-wavelength light source; 2) Beam conditioning optics; and, 3) Recording and reconstruction setup. The light source is a H_2 Raman shifter that is pumped by the 355 nm output beam of a pulsed Nd:YAG laser (Spectra Physics GCR-230-10) with a pulse duration of about 5 ns. The plane mirrors direct the pump beam into the H_2 Raman shifter. Lens *L1* (focal length, 50 cm) focuses the pump

laser beam into a Raman cell (length, 58 cm) that is filled with hydrogen gas (99.9999% purity). At the exit port of the cell is lens *L2* (focal length, 50 cm), which collimates the Raman output beams.

The Raman output beams are directed towards the beam conditioning section. The output beams of the Raman shifter consist of the following spectral components: Rayleigh (355 nm), Stokes (S_1, S_2, …) and anti-Stokes (aS_1, aS_2, …). The output beam energies depend on the hydrogen gas pressure in the Raman cell and on the pump energy (Garcia, W. et al., 2002). At a hydrogen gas pressure of 1.38 MPa and a pump energy of 6.5 mJ, the following Raman output lines (in nm) are obtained: 415.9 (S_1; blue), 502.9 (S_2; green), 635.9 (S_3; red), 864.5 (S_4), 309 (aS_1), 273.8 (aS_2), 245.8 (aS_3), and 222.9 (aS_4). The beam energy decreases with the Stokes (or anti-Stokes) number. The S_1 beam energy is 2.12 mJ which is 1.43 times greater than that of S_2 and 3.3 times higher than that of S_3. The Stokes beam energies are also larger than their anti-Stokes counterparts. For pulsed full-color digital holography, the first three Stokes output beams S_1 (blue), S_2 (green) and S_3 (red) are utilized as the primary additive color channels.

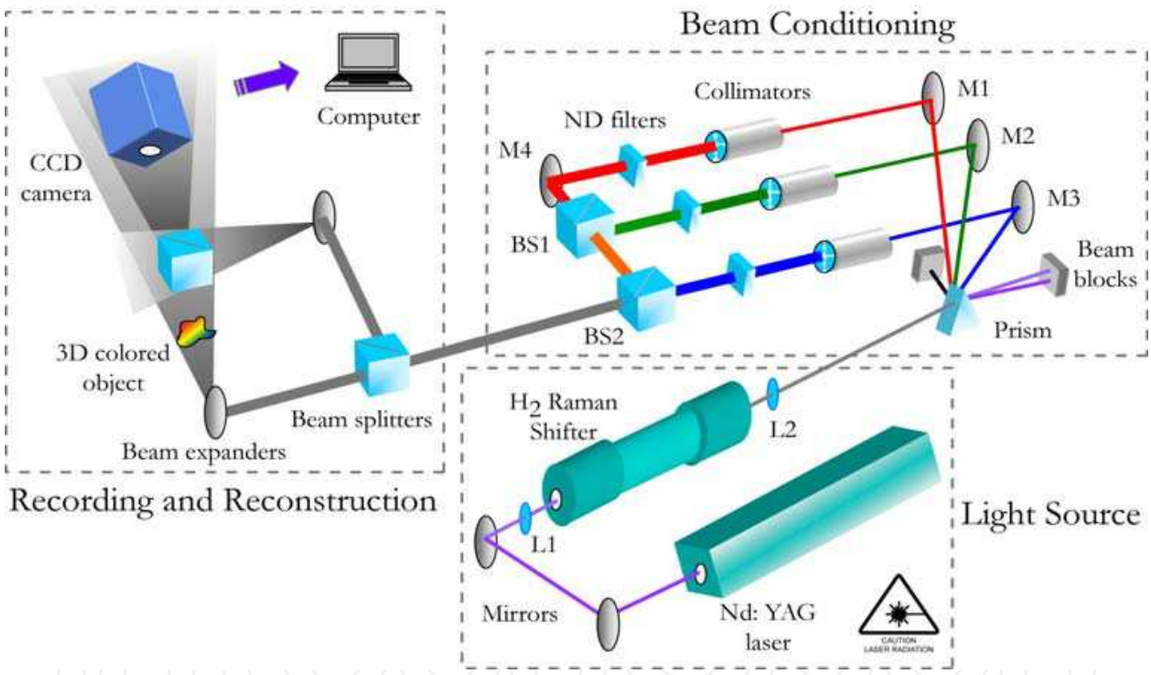

Fig. 1. Experimental setup for pulsed full-color digital holography.

3.2 Beam conditioning

To make the Raman shifter suitable for pulsed FCDH, we need to address the unequal relative energies and poor transverse intensity distributions of the S_1, S_2 and S_3 beams. The transverse intensity distribution of a Raman output beam is non-Gaussian. Uniform beam profiles and equal beam intensities are important for achieving uniform object illumination and better control of the beam ratio. Conditioning is required for the Stokes beams before they can be fully utilized as a holographic light source.

The beam-conditioning section consists of a Pellin-Broca prism, beam blocks, deflecting mirrors (*M1, M2, M3,* and *M4*), three sets of beam collimators, neutral density filters and

beam splitters (*BS1*, *BS2*). The prism disperses the output beams of the Raman shifter such that only the S_1, S_2 and S_3 beams are able to proceed to the collimators. The components of the collimators are not shown in Fig 1 for simplicity. Each collimator is composed of a first lens (focal length f = 11 cm, diameter d = 5.08 cm) that individually focuses the Stokes beams to spatial filters (d = 0.15 cm). The light that is transmitted by each filter is collimated by a second lens (f = 25 cm, d = 4.13 cm). The relative intensities of the collimated S_1, S_2 and S_3 beams are equalized with a set of neutral density filters (*ND* filters). The equalized Stokes beams are then recombined via mirror *M4* and beam splitters *BS1* and *BS2*. After *BS2*, the intensity of each Stokes beam has been reduced to 50 μW which is safe for the operation of the CCD camera (SONY XC-75, 640 x 480 pixels, monochrome). The recombined beams form the new holographic pulsed white light source.

Figure 2 demonstrates the benefits of beam conditioning on the beam profiles and relative intensities of the primary color channels from S_1, S_2 and S_3 Raman outputs. In Fig. 2(a) is an image of the selected Raman outputs before performing beam conditioning. The beam is characterized by the presence of intense high-frequency spatial structures and scattered color components. The beam intensity also exhibits temporal and spatial variations between pulses that are due to non-uniform gas heating in the Raman cell. These deleterious effects are minimized by the constructed beam conditioning section.

Figures 2(b) - 2(d) illustrate the improvement of the beam profiles and relative intensities which is 50 μW for each of the laser lines. Figure 2(e) presents the white light beam after superimposing the color channels (beam width ~ 2.54 cm). A slight chromatic dispersion remains in the superposition (manifested as halo) due to the wavelength dependence of beam divergence and chromatic aberration in the optics elements. We utilized the white light beam to record the RGB holograms of various test samples.

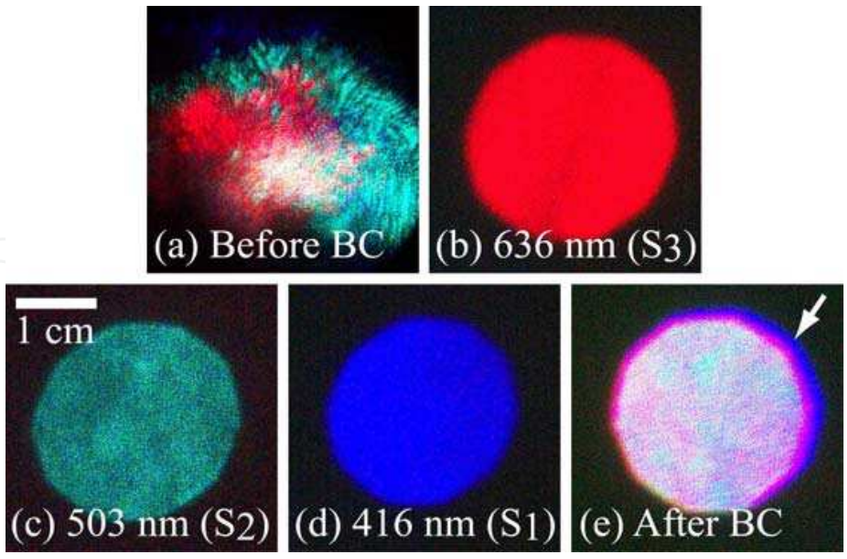

Fig. 2. Effects of beam conditioning (BC) on beam quality. (a) Before BC: overlapped S_1, S_2 and S_3 output beams of the Raman shifter. Uniform profiles and equalized intensities after BC for (b) S3; (c) S2; (d) S1 beams; and, (e) superposition of the beams. Arrow indicates the presence of a halo.

3.3 Recording and reconstruction

Hologram recording and reconstruction are performed with a typical in-line digital holographic setup. In the in-line configuration, the object and reference beams are approximately co-linear which result in widely-spaced interference fringes. Large fringes are ideal for enhanced CCD sampling. We adjusted the positions of the beam expanders (concave mirrors) for back illumination in the case of a transmitting object and for front illumination in the case of a reflecting opaque object. During hologram recording, the test object is illuminated, one beam at a time, by blocking the other two beams in the beam conditioning section. We used a negative resolution target as a transmitting test object and captured the interference of the object and reference beams with the CCD camera. The recorded *R*, *G* and *B* holograms produced by the S_3, S_2 and S_1 beams respectively, are resized, reconstructed, rendered with color and, finally, unified in the computer.

3.4 Resizing the holograms

Figure 3 depicts the resizing of the holograms based on the wavelength ratios. The original size of the *R*, *G* and *B* holograms is 480 x 640 pixels [Fig. 3(a) – 3(c)]. Figure 3(d) is the resized hologram for the *R* channel with new dimensions 734 x 979 pixels that is obtained after embedding the hologram in Fig 3(a) in a matrix with zero amplitude. We obtained the new dimensions by applying Eqn. 2.2 in both the vertical and horizontal directions with λ_2 = 636 nm and λ_1 = 416 nm.

Figure 3(e) is the resized hologram for the green channel with new dimensions 581 x 774 pixels. The new dimensions are obtained by applying Eqn. 2.2 in the vertical as well as in the horizontal direction with λ_2 = 503 nm and λ_1 = 416 nm. The blue hologram retains its original dimensions.

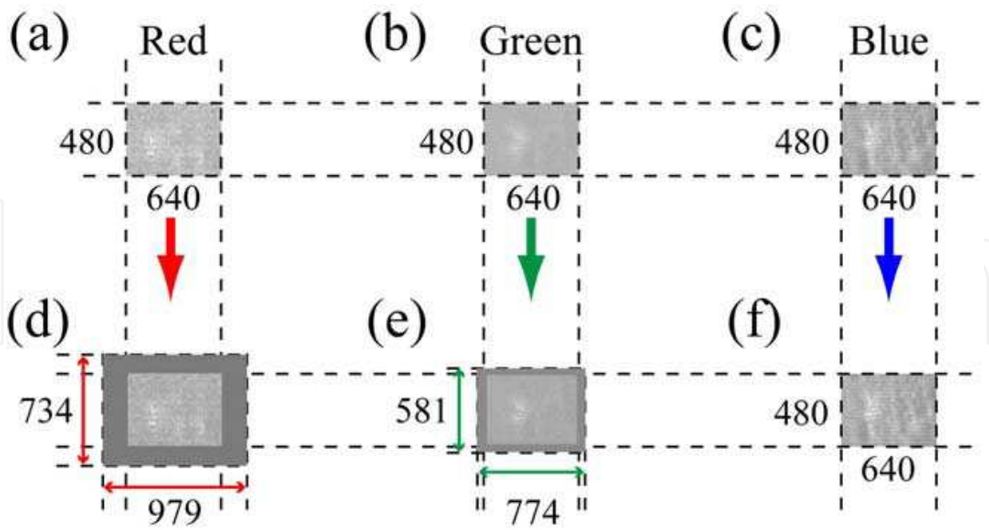

Fig. 3. Resizing of the color holograms. Original size of the (a) red, (b) green and (c) blue holograms with dimensions 480 pixels (V) x 640 pixels (H). (d) and (e) are the resized red and green holograms, respectively, with new dimensions indicated. Blue hologram retains its original dimensions.

3.5 Reconstruction of holograms

The *B* hologram and the resized *R* and *G* holograms are reconstructed at distances where the images are best focused. The distance of the best-focused image is established by numerically focusing the hologram at various distances and then selecting the sharpest image.

For the purposes of comparison, reconstructions from resized holograms are also plotted at the same reconstruction distance (Ferraro et al., 2004). The fixed distance condition corresponds to the reconstruction distance of the blue channel. The *RGB* reconstructions are then compared in terms of size and resolution.

4. Control of chromatic dispersion

4.1 Wavelength dependence of image parameters

Figure 4 shows the recorded holograms and the test object used. In Figs. 4(a) to 4(c) are the recorded *R*, *G* and *B* holograms, respectively. The test object is an element number "5" of the negative resolution target with a height of 4 mm. Figure 4(d) is an image of the test object that is illuminated by the Raman white light source. The *RGB* holograms are then evaluated using the Fresnel method using the respective recording wavelengths. The lens-like nature of holograms results in the focusing of the incident reconstruction beam forming an image. The image size, lateral resolution and longitudinal resolution are investigated for their wavelength dependences.

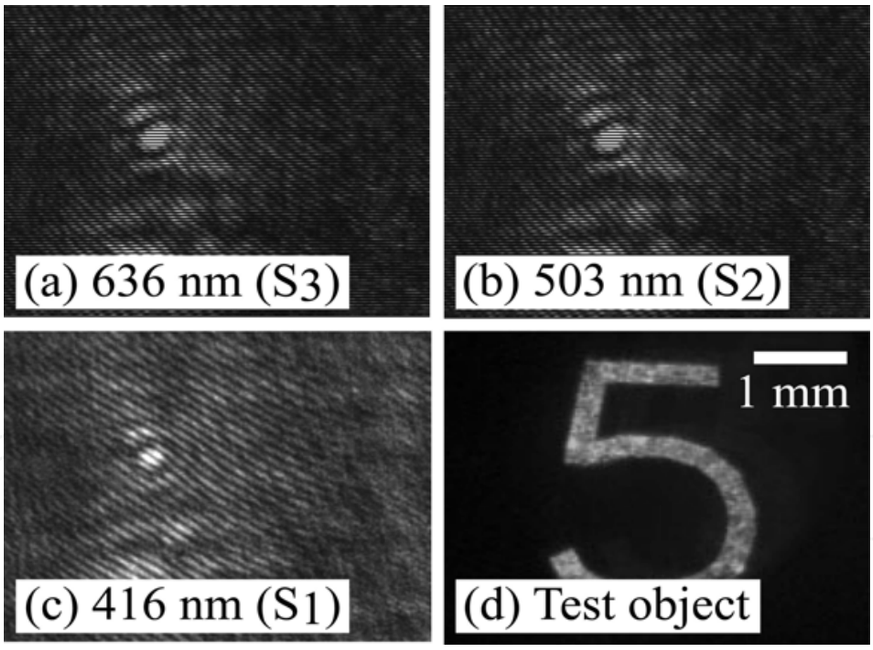

Fig. 4. Recorded holograms. (a) Red, (b) green and (c) blue holograms of the transmitting test object shown in (d).

Figure 5 presents a matrix of the color reconstructions that reveal the effects of wavelength and object-to-CCD recording distance (*z*) on the image size. For a fixed distance, down a column, the image size increases with decreasing wavelength. For a constant wavelength, moving from left to right, the image size decreases as distance increases. The results demonstrate that the image size increases with decreasing wavelength.

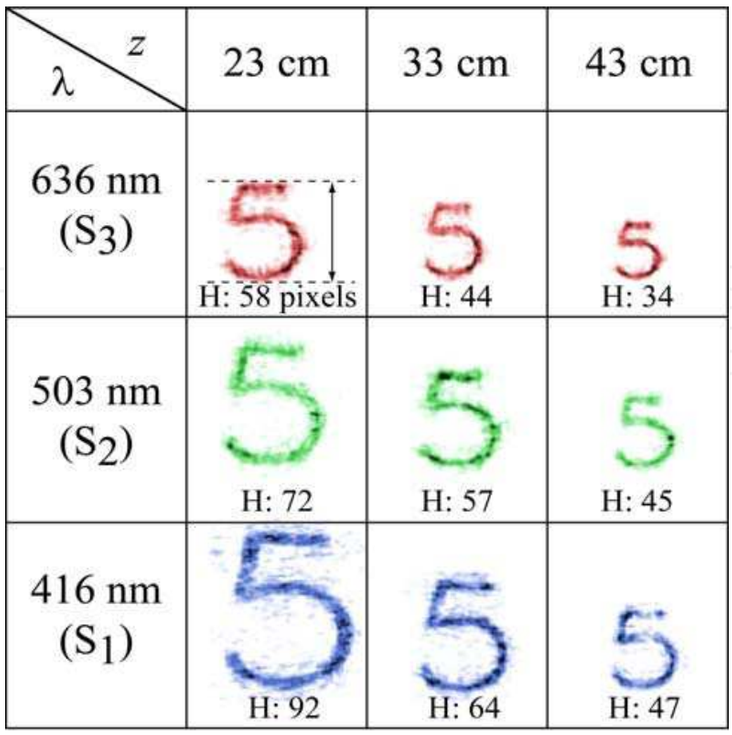

Fig. 5. Dependences of the image size on illumination wavelength and object-to-CCD distance (z) during recording. Evaluation of the color reconstructions is based on image height (H, in number of pixels).

Figure 6 illustrates the effects of the light source wavelength on the longitudinal (axial) resolution of the reconstructions. At a particular wavelength, an intensity line scan is obtained across an array of reconstructions plotted at equally-spaced axial positions. Figure 6(a) shows the arrays of *RGB* reconstructions from holograms recorded at the same object-to-CCD distance. The intensity line scans are obtained through the middle portions of the number "5" and then are plotted at the different axial distances.

Figures 6(b) - 6(d) show the intensity scans for the *R*, *G* and *B* arrays, respectively. To estimate how fast a focused image blurs with axial distance, here we considered the distance range (Δz) where the intensity decreases to half its maximum value. The intensity scan for the red reconstructions [Fig. 6(b)] exhibits slower change across the axial direction (Δz = 15 cm). While the blue reconstructions [Fig 6(d)] exhibit faster change in intensity (Δz = 7.5 cm). The results demonstrate that the longitudinal resolution increases with shorter wavelengths. The reconstructions from the blue hologram is said to have a narrow depth of focus while those from the red hologram have a larger depth of focus.

Lateral resolution also improves at shorter wavelengths as illustrated in Fig. 5 where the images are larger for the case of blue reconstructions. A larger reconstructed image of an object would reveal more details – an observation that is consistent with the wavelength dependence of the pixel size in the image plane. Since each image pixel represents a range of spatial frequencies (by virtue of the Fourier transformation) a bigger reconstruction can also be interpreted as a representation of higher spatial frequencies that contain the finer details of the object.

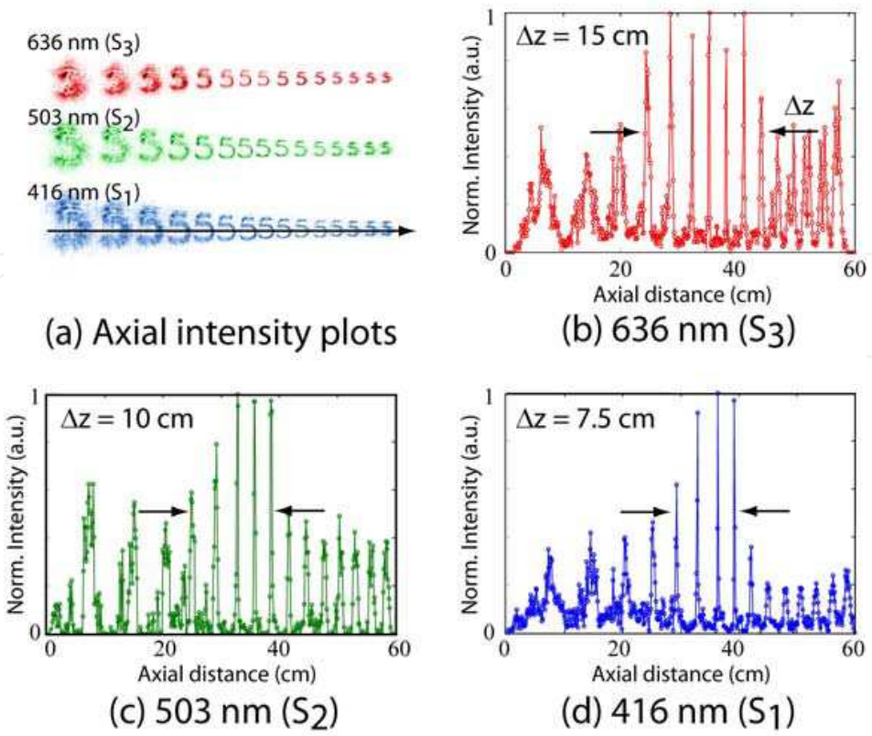

Fig. 6. Dependence of longitudinal (axial) resolution of the reconstructions on illumination wavelength. (a) Arrays of *RGB* reconstructions plotted at equally-spaced axial positions. The arrowed line indicates the scanned portions across an array. (b), (c) and (d) are the axial intensity line scans for the *R*, *G* and *B* reconstructions, respectively. Based on the range (Δz) where intensity decreases to half its maximum, the narrowest depth of focus (highest axial resolution) is observed in the reconstructions at the shortest wavelength (416 nm, S_1) (d).

4.2 Proper fit of the color reconstructions

Chromatic dispersion of the superimposed reconstructions can be controlled by resizing the holograms and reconstructing at best-focused distances. Figure 7 demonstrates the effects of hologram resizing on the size and resolution of the superimposed *RGB* reconstructions.

Figure 7 sub-panels (a) - (c) are the *RGB* reconstructions from the original size holograms. The heights of the reconstructions are 53 pixels, 65 pixels and 76 pixels, for *R*, *G*, and *B* channels, respectively. The superimposed image reconstruction [Fig. 7(d)] evidently demonstrates the wavelength dependences of the image size. The reconstruction distances where the images are best focused are 22.0 cm, 21.0 cm and 20.5 cm for *R*, *G*, and *B* reconstructions, respectively. The variance of the image distance can be attributed to chromatic aberrations in the optics used.

Figure 7 sub-panels (e) – (g) are the reconstructions from the resized holograms and plotted using a fixed image distance of 20.5 cm (chosen from image distance of the blue color channel). The images are successfully resized but the heights are not exactly equalized as depicted in the superimposed image [Fig. 7(h)]. The heights of the reconstructions are 81 pixels, 73 pixels and 76 pixels for *R*, *G*, and *B* channels, respectively. Such an unsatisfactory result could be attributed to the assumption that the location of the image does not vary significantly with wavelength.

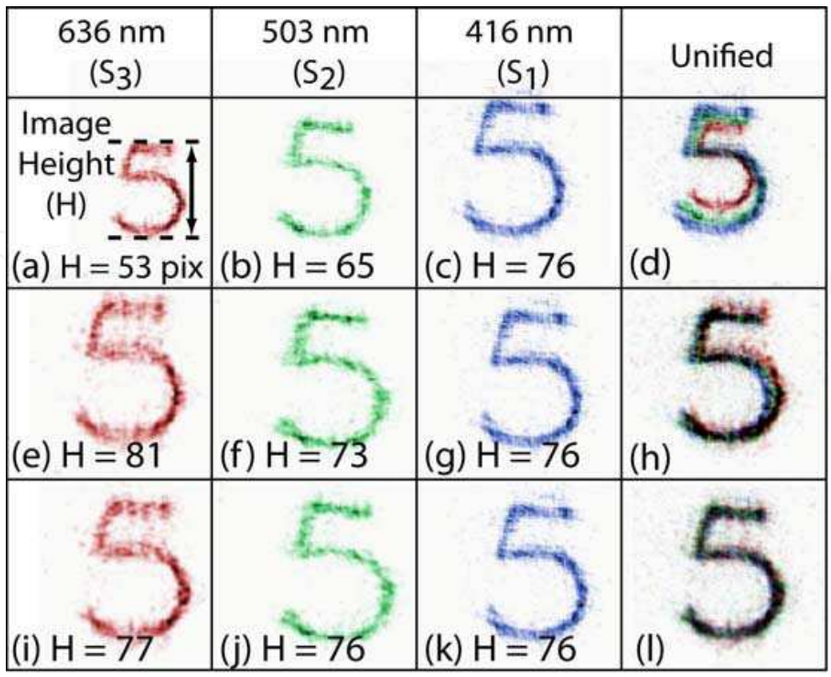

Fig. 7. Control of chromatic dispersion. (a) – (d) *RGB* reconstructions and unified image using holograms at original size. (e) – (h) Reconstructions from resized holograms and plotted at a fixed image distance. (i) – (l) Reconstructions from resized holograms and plotted at best-focused image distances.

Figures 7 sub-panels (i) – (k) are the reconstructions obtained from resized holograms using image distances of 22.0 cm, 21.0 cm and 20.5 cm for the *R*, *G*, and *B* channels, respectively. The heights of the reconstructions are 77 pixels, 76 pixels and 76 pixels for *R*, *G*, and *B* channels respectively. The heights are more uniform when the image distances that are utilized correspond to those of the best focused images. The small variance that has remained in the heights of the reconstructions is attributed to the depth of focus where the image is acceptably focused. Proper fit of the RGB reconstructions is achieved after resizing the holograms based on wavelength ratios and reconstructing at best-focused image distances [Fig. 7(l)].

Figure 8 demonstrates the improvement of the fit of the full-color reunified image after application of the resizing technique. Figure 8(a) presents the intensity line scan across a portion of the superposed reconstructions obtained without resizing the holograms. At this stage, the RGB channels are unsuitable for unification as evident from the split lines corresponding to a solid portion of the number "5". Figure 8(b) shows the line scan for the unified image after resizing the holograms at a fixed image distance. The presence of bifurcation in the intensity scan indicates a poor fit of the *RGB* channels after the reconstructing at a fixed distance. Figure 8(c) presents the line scan of the unified image after hologram resizing and plotting at the best-focused image distances. The smooth intensity scan demonstrates proper fit of the *RGB* channels when the holograms are resized based on wavelength ratios and reconstructed at best-focused image distances.

Figure 9 conveys the importance of hologram resizing on the longitudinal resolution. Figure 9(a) presents a horizontal array of full-color reconstructions in the absence of hologram resizing. The reconstructions are plotted at equally-spaced axial planes in the foreground and background of the best focused image planes. We used the contrast of the intensity profile as a measure of the axial resolution. High contrast in the axial intensity plot within a short axial range would mean enhanced localization of the colored test object.

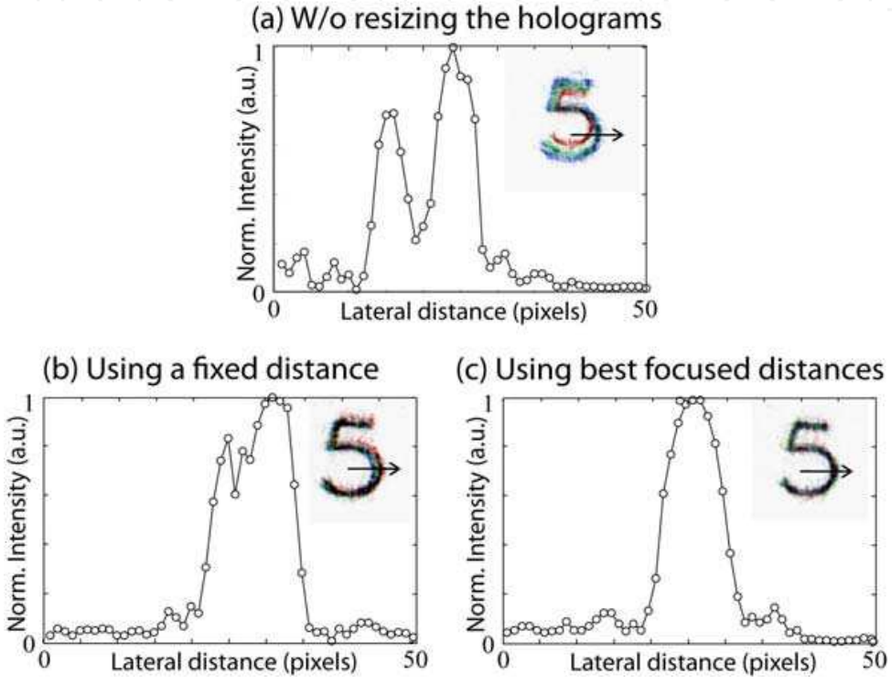

Fig. 8. Intensity line scans to demonstrate the effects of hologram resizing on the proper fit of the *RGB* reconstructions. (a) Without hologram resizing. (b) With hologram resizing and reconstruction at a fixed distance. (c) With hologram resizing and reconstruction at best-focused image distances.

Figure 9(b) shows the horizontal intensity line scan across the array in Fig. 9(a). The line scan passes through the mid portion of the reconstructed images of "5" as indicated by the arrowed line in Fig. 9(a). The intensity profile has a low contrast (difference between maximum and minimum intensity values as depicted by the circles) and exhibits a gradual change across the array. Figure 9(c) shows an array of full-color reconstructions after resizing the holograms. The high contrast in the intensity profile [Fig. 9(d)] indicates an improvement of the longitudinal or axial resolution as a result of the hologram resizing. Enhanced axial resolution is important in optical sectioning where a specific plane of a three dimensional scene has to be accessed. The full-color reconstruction must exhibit high longitudinal resolution or narrow depth of focus in order to resolve the various axial planes.

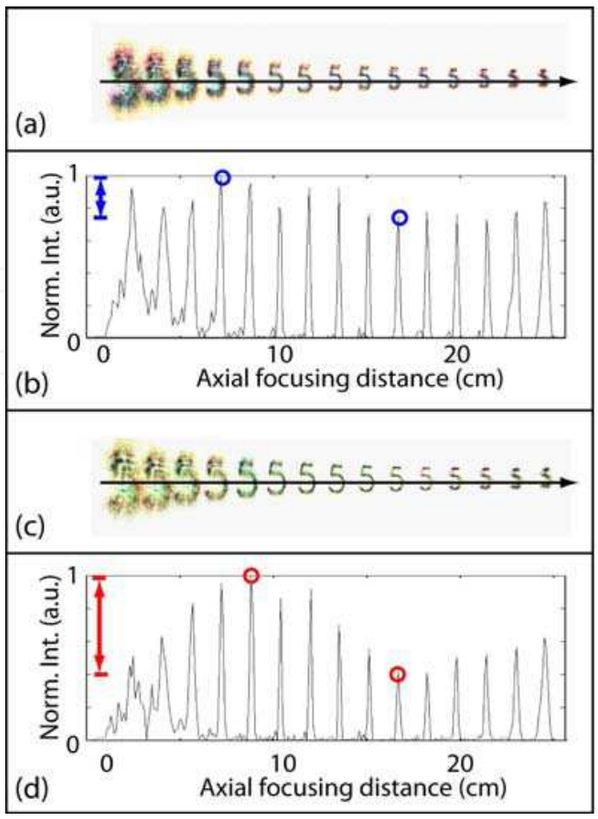

Fig. 9. Effects of hologram resizing on longitudinal resolution. (a) Array of full-color reconstructions without hologram resizing. (b) Intensity scan across the array in (a) shows low contrast and gradual change. (c) Full-color reconstructions from resized holograms. (d) Intensity scan across the array in (c) shows high contrast and rapid change demonstrating enhanced axial resolution.

5. Summary and conclusions

We have discussed pulsed FCDH with a hydrogen Raman shifter as the single source of pulsed, highly-directional multi-wavelength light. The first three Stokes beam outputs (λ_{S1} = 415.9 nm, λ_{S2} = 502.9 nm, λ_{S3} = 635.9 nm) of the Raman shifter are utilized as the three primary color channel for carrying all the color information from the object. A simple beam conditioning procedure for improving the beam quality of the Stokes beams and for equalizing their beam was developed and implemented and holographic recording and reconstruction were both successfully demonstrated. The Raman shifter is a promising light source for pulsed FCDH because it is inexpensive to construct and maintain.

The usefulness of full color holograms depends on the quality and resolution of the reconstructed images. Higher resolution and narrower depth of focus are gained for reconstructions from holograms that are recorded at shorter wavelengths. The wavelength dependence of the image size and resolution spatially disperses the reconstructions from the primary color channels resulting in blurred unacceptable image. Compensation for color dispersion could be done by resizing the holograms using the ratio of wavelengths and reconstructing at a fixed image distance. However, the wavelength dependence of the beam

divergence and optical aberrations result in the spatial displacement of the point reference beam that directly changes the direction and shape of the reference beam and therefore, the image distance. Knowledge of the variance in the image distance for the primary color channels, has allowed us to rescale using the image distance that yielded the best focused image thereby assuring better compensation of size, resolution and depth of focus.

6. Acknowledgments

We acknowledge the financial support of PCASTRD-DOST and OVCRD-UP Diliman. We also thank M. Cadatal, F. Daquiado, S. Ledesma, M. Francisco, I. Quiatchon, R. Ibarreta, J. Palero and C.A. Alonzo of NIP for their valuable technical assistance in the various stages of the FCDH work.

7. References

[1] Almoro, P., Cadatal, M., Garcia, W. & Saloma, C. (2004). Pulsed multicolor digital holography with hydrogen Raman shifter. Appl Opt. 43, 2267-2271.

[2] Almoro, P., Garcia, W. & Saloma, C. (2007). Colored object recognition by digital holography and a hydrogen Raman shifter. Opt Express 15, 7176-7181.

[3] Andreeva, O.V. (2002). Proposals for a terminological dictionary of optics. Holography, J. Opt. Technol. 69 , 367-374.

[4] Bates, H. (1973). Burst-Mode Frequency-Doubled YAG:Nd3+ Laser for Time-Sequenced High-Speed Photography and Holography. Appl. Opt. 12, 1172-1178.

[5] Benton, S.A. (2002). Holography reinvented, Proc. SPIE 4737, 23-26.

[6] Bjelkhagen, H. I. & Vukicevic, D. (2002). Color holography: a new technique for reproduction of paintings. Proc. SPIE 4659, 83-90.

[7] Bjelkhagen, H. I. (2002). Super-realistic imaging based on color holography and Lippmann photography. Proc. SPIE 4737, 131-141.

[8] Colomb, T., Pavillon, N., Kühn, J., Cuche, E., Depeursinge, C., & Emery, Y. (2010). Extended depth-of-focus by digital holographic microscopy. Opt. Lett. 35, 1840-1842.

[9] Desse, J., Albe, F. & Tribillon, J. (2002). Real-time color holographic interferometry. Appl. Opt. 41, 5326-5333.

[10] Demoli, N., Vukicevic, D. & Torzynski, M. (2003). Dynamic digital holographic interferometry with three wavelengths. Opt. Express 11, 767-774.

[11] Ferraro, P., De Nicola, S., Coppola, G., Finizio, A., Alfieri, D. & Pierattini, G. (2004). Controlling image size as a function of distance and wavelength in Fresnel-transform reconstruction of digital holograms. Opt. Lett. 29, 854-856.

[12] Garcia, J., Mas, D. & Dorsch, R. (1996). Fractional-Fourier-transform calculation through the fast-Fourier-transform algorithm. Appl. Opt. 35, 7013-7018.

[13] Garcia, W., Palero, J. & Saloma, C. (2001). Temporal coherence control of Nd:YAG pumped Raman shifter. Opt. Commun. 97, 109-114.

[14] Goodman, J. (1996). Introduction to Fourier Optics. 2nd ed., McGraw-Hill, Singapore.

[15] Gustafsson, J. (2000). Finding new wavelengths for pulsed holography. Proc. SPIE 4149, 353-358.

[16] Harthong, J., Sadi, J., Torzynski, M. & Vukicevic, D. (1997). Speckle phase averaging in high-resolution color holography. J. Opt. Soc. Am. A 14, 405-410.
[17] Javidi B., & Tajahuerce, E. (2000). Three-dimensional object recognition by use of digital holography. Opt. Lett. 25, 610-612.
[18] Jeong, T. H., Bjelkhagen, H. I. & Spoto, L. (1999). Holographic interferometry with multiple wavelengths. Appl. Opt. 36, 3686-3688.
[19] Kreis, T. (2002). Frequency analysis of digital holography with reconstruction by convolution. Opt. Eng. 41, 1829-1839.
[20] Kubota, T., Takabayashi, E., Kashiwagi, T., Watanabe, M., & Ueda, K. (2001). Color reflection holography using four recording wavelengths. Proc. SPIE 4296, 126-133.
[21] Kubota, T. & Ose, T. (1979). Lippmann color holograms recorded in methylene-bluesensitized dichromated gelatine. Opt. Lett. 4, 289-291.
[22] Kubota, T. (1986). Recording of high quality color holograms. Appl. Opt. 25, 4141-4145.
[23] Leith, E. N., Lyon, P., & Chen, H., (1991). Imaging problems with femtosecond-pulse holography. J. Opt. Soc. Am. A 8, 1014-1018.
[24] Lin, L., & LoBianco, C. (1967). Experimental Techniques in Making Multicolor White Light Reconstructed Holograms. Appl. Opt. 6, 1255-1258.
[25] Liu, Z., Centurion, M., Panotopoulos, G., Hong, J., & Psaltis, D. (2002). Holographic recording of fast events on a CCD camera. Opt. Lett. 27, 22-24.
[26] Mallick, S. (1975). Pulse Holography of Uniformly Moving Objects. Appl. Opt. 14, 602-605.
[27] Olivares-Perez, A., Berriel-Valdos, L. & Morales, A. (1989). Magnification effect and color blur behavior in holography. Appl. Opt. 28, 4366-4369.
[28] Pedrini, G., Gusev, M., Schedin, S., & Tiziani, H. J. (2003). Pulsed digital holographic interferometry by using a flexible fiber endoscope. Opt. Lasers Eng. 40, 487-499.
[29] Pedrini, G., Schedin, S., & Tiziani, H. J. (2002). Pulsed digital holography combined with laser vibrometry for 3D measurements of vibrating objects. Opt. Lasers Eng. 38, 117-129.
[30] Peercy, M., & Hesselink, L. (1994). Wavelength selection for true-color holography. Appl. Opt. 33, 6811-6817.
[31] Schnars U. & Jüptner W. (2002). Digital recording and numerical reconstruction of holograms, Meas. Sci. Technol. 13, R85-R101.
[32] Schulze, M. A., Hunt, M., Voelkl, E., Hickson, J., Usry, W., Smith, R., Bryant R. & Thomas Jr., C. (2003). Semiconductor wafer defect detection using digital holography, Proc. SPIE 5041, 183-`193.
[33] Seebacher, S., Osten, W., Baumbach, T., & Jüptner, W. (2001). The determination of material parameters of micro-components using digital holography. Opt. Lasers Eng. 36, 103-126.
[34] Upatnieks, J., (1979) Image Formation. Handbook of Optical Holography. Caulfield, H. (Ed.), New York.
[35] Wedendal, P. R. & Bjelkhagen, H. I. (1974). Dynamics of Human Teeth in Function by Means of Double Pulsed Holography; an Experimental Investigation. Appl. Opt. 13, 2481-2485.

[36] Yamaguchi, I., Matsumura, T. & Kato, J. (2002). Phase-shifting color digital holography. Opt. Lett. 27, 1108-1110.
[37] Zhang, T. & Yamaguchi, I., (1998). Three-dimensional microscopy with phase-shifting digital holography. Opt. Lett. 23, 1221-1223.

Holography, Research and Technologies

Edited by Prof. Joseph Rosen

ISBN 978-953-307-227-2
Hard cover, 454 pages
Publisher InTech
Published online 28, February, 2011
Published in print edition February, 2011

Holography has recently become a field of much interest because of the many new applications implemented by various holographic techniques. This book is a collection of 22 excellent chapters written by various experts, and it covers various aspects of holography. The chapters of the book are organized in six sections, starting with theory, continuing with materials, techniques, applications as well as digital algorithms, and finally ending with non-optical holograms. The book contains recent outputs from researches belonging to different research groups worldwide, providing a rich diversity of approaches to the topic of holography.

How to reference

In order to correctly reference this scholarly work, feel free to copy and paste the following:

Percival Almoro, Wilson Garcia and Caesar Saloma (2011). Pulsed Full-Color Digital Holography with a Raman Shifter, Holography, Research and Technologies, Prof. Joseph Rosen (Ed.), ISBN: 978-953-307-227-2, InTech, Available from: http://www.intechopen.com/books/holography-research-and-technologies/pulsed-full-color-digital-holography-with-a-raman-shifter

INTECH
open science | open minds

InTech Europe
University Campus STeP Ri
Slavka Krautzeka 83/A
51000 Rijeka, Croatia
Phone: +385 (51) 770 447
Fax: +385 (51) 686 166
www.intechopen.com

InTech China
Unit 405, Office Block, Hotel Equatorial Shanghai
No.65, Yan An Road (West), Shanghai, 200040, China
中国上海市延安西路65号上海国际贵都大饭店办公楼405单元
Phone: +86-21-62489820
Fax: +86-21-62489821

IntechOpen